PERGAMON

International Journal of Solids and Structures 38 (2001) 833–853

INTERNATIONAL JOURNAL OF SOLIDS and STRUCTURES

www.elsevier.com/locate/ijsolstr

Plastic flow in a composite: a comparison of nonlocal continuum and discrete dislocation predictions

J.L. Bassani [a], A. Needleman [b,*], E. Van der Giessen [c]

[a] *Department of Mechanical Engineering and Applied Mechanics, University of Pennsylvania, Philadelphia, PA 19104, USA*
[b] *Division of Engineering, Brown University, Providence, RI 02912, USA*
[c] *Koiter Institute Delft, Delft University of Technology, Mekelweg 2, 2628 CD Delft, Netherlands*

Received 13 June 1999; in revised form 7 March 2000

Abstract

A two-dimensional model composite with elastic reinforcements in a crystalline matrix subject to macroscopic shear is considered using both discrete dislocation plasticity and a nonlocal continuum crystal plasticity theory. Only single slip is permitted in the matrix material. The discrete dislocation results are used as numerical experiments, and we explore the extent to which the nonlocal crystal plasticity theory can reproduce their behavior. In the nonlocal theory, the hardening rate depends on a particular strain gradient that provides a measure of plastic (or elastic) incompatibility. This nonlocal formulation preserves the classical structure of the incremental boundary value problem. Two composite morphologies are considered; one gives rise to relatively high composite hardening and a dependence of the stress–strain response on size while the other exhibits nearly ideally plastic composite response and size independence. The predictions of the nonlocal plasticity model are confronted with the results of the discrete dislocation calculations for the overall composite stress–strain response and the phase averages of stress. Material parameters are found with which the nonlocal continuum plasticity formulation predicts trends that are in good accord with the discrete dislocation plasticity simulations.

Keywords: Plastic flow; Discrete dislocation

1. Introduction

There is a considerable body of experimental evidence (Ebeling and Ashby, 1966; Brown and Ham, 1971; De Guzman et al., 1993; Fleck et al., 1994; Ma and Clarke, 1995; Stölken and Evans, 1998), which shows that inhomogeneous plastic flow in crystalline solids is inherently size dependent over a scale that ranges from a fraction of a micron to a hundred microns or so – with the smaller being harder. Already many years ago, the connection between size dependence and gradients of plastic deformation was made through the notion of incompatibility, which is characterized by a certain spatial gradient of the plastic (or elastic) distortion (Bilby et al., 1955; Kröner and Seeger, 1959; Nye, 1953). This notion can be related to the more

* Corresponding author. Tel.: +1-401-863-2863; fax: +1-401-863-1157.
E-mail address: needle@engin.brown.edu (A. Needleman).

0020-7683/01/$ - see front matter
PII: S0020-7683(00)00059-7

physical concept of a dislocation density tensor and to the geometrically necessary dislocations. What remains to be determined is how to incorporate that incompatibility measure into a continuum description of plastic flow. In Acharya and Bassani (1996, 2000), the incompatibility measure is incorporated directly into the hardening description. Arsenlis and Parks (1999) have developed another nonlocal plasticity theory in which a factor relating the density of geometrically necessary dislocations to plastic strain gradients is introduced, while Fleck and Hutchinson (1993) used incompatibility to motivate a nonlocal continuum formulation involving higher order stresses. Gurtin (2000) has proposed an approach in which the gradient of plastic deformation is used to introduce microstresses. The precise implementation has a major effect on the nature of the resulting boundary value problem. The correctness of these approaches will ultimately be decided through a comparison of their predictions with experiment. However, detailed comparisons between the predictions of continuum plasticity with a direct dislocation based description of plastic flow will be useful in assessing the various nonlocal formulations.

As a specific example, plastic flow of a model metal–matrix composite, with the reinforcements embedded in an individual grain is considered. Attention is focused on two commonly observed characteristics of the behavior of metal–matrix composites which are not amenable to explanation based on conventional, size-independent plasticity theory (e.g. Nan and Clarke, 1996): (i) the stress–strain behavior is size dependent for reinforcement sizes in the micron range; and (ii) the matrix stress–strain behavior that needs to be assumed in calculations to get good agreement with experiment typically differs from the observed stress–strain behavior of the unreinforced material. Discrete dislocation plasticity predictions are consistent with these observations (Cleveringa et al., 1997, 1998). Size-dependent response emerges from the development of a structure of geometrically necessary dislocations (Ashby, 1970) and smaller reinforcement sizes, in the range of tenths of microns to tens of microns, lead to harder overall response, which is consistent with the experimental observations (Ebeling and Ashby, 1966; Brown and Ham, 1971). Whether or not geometrically necessary dislocations are present for a given loading history depends on the composite morphology (Cleveringa et al., 1997). Also, the response of the composite matrix can be different from that of the homogeneous material because of the different dislocation structures that develop.

In this study, we compare the predictions of the nonlocal plasticity theory of Acharya and Bassani (1996, 2000) with the discrete dislocation predictions of Cleveringa et al. (1997, 1998) for a two-dimensional model, composite material with periodic rectangular reinforcements. The composite is subject to plane strain simple shear with the crystal axes such that the matrix deforms in single slip. The theory of Acharya and Bassani (1996, 2000) is based on the hypothesis that the incompatibility directly influences the hardening behavior of a single crystal. In their 'simple theory', a particular strain gradient, which is taken to be a measure of elastic (or plastic) incompatibility, enters the flow rule only through the instantaneous hardening rate. Consequently, the classical structure of incremental boundary value problems (Hill, 1958) is preserved so that higher-order stresses and additional boundary conditions are not required. As a result, standard finite-element formulations based upon purely local constitutive response, such as the single crystal formulation in Peirce et al. (1983), are readily extended to incorporate this simple theory. Still, a material length scale enters the hardening relation on dimensional grounds. For a particular constitutive relation, the relative magnitudes of this material scale and the microstructural length scales, e.g. particle size, determine the response for a particular composite morphology.

In the discrete dislocation formulation (Van der Giessen and Needleman, 1995; Cleveringa et al., 1997), the dislocations are modeled as line defects in a linear elastic solid. Attention is restricted to small strains, and the stress, strain and displacement fields are written as superpositions of fields due to the discrete dislocations, which are singular inside the body, and complementary (image) fields that enforce the boundary conditions. This leads to a linear elastic boundary value problem for the smooth complementary fields which is solved by the finite-element method. Thus, the long range interactions between dislocations are accounted for through the continuum elasticity fields. Drag during dislocation motion, interactions with obstacles, and dislocation nucleation and annihilation are also accounted for. These are not represented by

the elasticity description of dislocations and are incorporated into the formulation through a set of constitutive rules which are based on those proposed by Kubin et al. (1992).

Results are presented for two of the three composite morphologies investigated by Cleveringa et al. (1997). In one of the morphologies, slip cannot propagate across the unit cell because it is blocked by the elastic reinforcement. In this case, the composite exhibits strong strain hardening and the overall stress–strain response is strongly size dependent. In the other morphology, there is a channel of material, where slip can propagate unimpeded across the cell. For this composite morphology, deformation is focused in a slip band, and the discrete dislocation calculations give rise to a slightly softening stress–strain response that is not size dependent. The challenge for the nonlocal plasticity calculations is to predict, for matrix plastic flow properties being specified for one reinforcement size and morphology, both the size and morphology dependence of the overall composite response.

2. Problem formulation

The calculations are carried out within the context of a small displacement gradient formulation. Cartesian tensor notation is used throughout. With geometry changes neglected, the principle of virtual work is written as

$$\int_V \sigma_{ij}\,\delta\epsilon_{ij}\,\mathrm{d}V = \int_S T_i\,\delta u_i\,\mathrm{d}S, \tag{1}$$

where σ_{ij} are the stress tensor components, u_i are the displacement field components, V and S are the volume and surface area of the body, respectively, and

$$T_i = \sigma_{ij} v_j, \tag{2}$$

$$\epsilon_{ij} = \tfrac{1}{2}\left(u_{i,j} + u_{j,i}\right) \tag{3}$$

with v_i being the components of the surface normal and $(\ )_{,i}$ denoting partial differentiation with respect to x_i.

A two-dimensional model composite material containing elastic rectangular particles in a plastically deforming matrix is analyzed. The particles are arranged in a doubly periodic hexagonal array as shown in Fig. 1. Each unit cell is of width $2w$ and height $2c$ ($w/c = \sqrt{3}$) and contains two particles of size $2w_f \times 2c_f$, one being located at the center of the cell. Two morphologies are considered, which have the same area fraction, $f = 0.2$, of reinforcing particles: material (i) contains square particle ($c_f = w_f$, $c_f = 0.416c$), thus leaving a channel of unreinforced material, while material (iii) has particles with an aspect ratio of 2 ($c_f = 2w_f$, $c_f = 0.588c$) so that all slip planes are blocked by particles; the identification of the composite morphologies follows that in Cleveringa et al. (1997, 1998).

The unit cell is subjected to plane strain and simple shear. The shearing direction is the x_1-direction so that the boundary conditions are expressed by

$$u_1(t) = \pm c\Gamma, \quad u_2(t) = 0 \quad \text{along } x_2 = \pm c, \tag{4}$$

where $\Gamma(t)$ is the applied shear at time t. Periodic boundary conditions are imposed along the lateral sides $x_1 = \pm w$. Although these boundary conditions constrain the rotation of the particles at the cell vertices (Fig. 1), the resulting boundary value problem is computationally more convenient than one using the most general periodic conditions consistent with the overall simple shear. For small strains, the dependence of the response on composite morphology will not be affected by the additional constraint.

The average shear stress τ_{ave} needed to sustain the deformation is computed from the shear stress σ_{12}, either along the top or the bottom face of the cell:

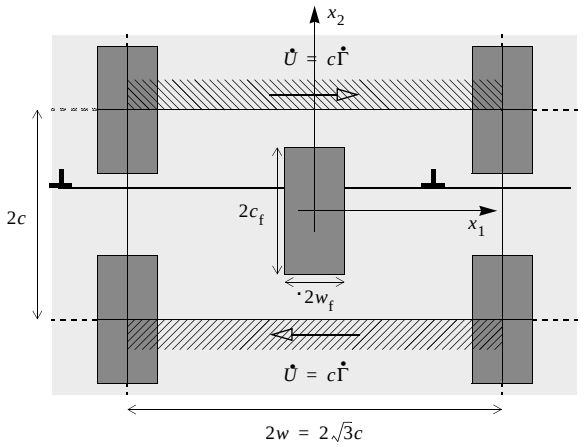

Fig. 1. Unit cell of a composite material with a doubly periodic array of elastic particles. All slip planes are taken to be parallel to the applied shear direction (x_1).

$$\tau_{\text{ave}} = \frac{1}{2w}\int_{-w}^{w} \sigma_{12}(x_1, \pm c)\,\mathrm{d}x_1. \tag{5}$$

Predictions of the discrete dislocation and the nonlocal crystal plasticity formulations are compared for the overall composite response and for the average fields that develop within each phase. The elastic properties are the same in both types of analyses, and identical to those used in Cleveringa et al. (1997, 1998). Each phase is taken to be elastically isotropic, with shear modulus $\mu = 26.3$ GPa and Poisson's ratio $\nu = 0.33$ for the matrix. The corresponding values for the reinforcement are 192.3 GPa and 0.17, respectively. These values are representative for silicon carbide particles in an aluminum matrix.

2.1. Discrete dislocation plasticity

In a discrete dislocation plasticity description, dislocations are represented as line defects in a linear elastic continuum (Nabarro, 1967; Hirth and Lothe, 1968). The formulation used here falls within the framework of Van der Giessen and Needleman (1995), which is fully three dimensional. Applications to date have been restricted to two dimensional boundary value problems, for both single slip, (Cleveringa et al., 1997), and multiple slip (Cleveringa et al., 1999). Only a brief summary is given here in the context of two dimensions and single slip; further details and a description of the general framework may be found in these references.

The computation of the deformation history is carried out in an incremental manner. Each time step Δt involves three main computational stages: (i) determining the forces on the dislocations, i.e. the Peach–Koehler force; (ii) determining the rate of change of the dislocation structure, which involves the motion of dislocations, the generation of new dislocations, their mutual annihilation, and their pinning at obstacles; and (iii) determining the stress and strain state for the current dislocation arrangement.

In this study, only edge dislocations on a single slip system are considered, with the slip plane normal being in the x_2-direction and with the glide direction being in the x_1-direction. All dislocations have the same Burgers vector magnitude b (the value $b = 2.5 \times 10^{-10}$ m is used in the calculations here). Under these circumstances, the Peach–Koehler force on the kth dislocation, $f^{(k)}$, is simply

$$f^{(k)} = \sigma_{12}^{(k)} b. \tag{6}$$

The magnitude of the glide velocity $v^{(k)}$ of dislocation k is taken to be linearly related to the Peach–Koehler force through the drag relation

$$f^{(k)} = Bv^{(k)}, \tag{7}$$

where B is the drag coefficient, with $B = 10^{-4}$ Pa s taken as a representative value for aluminium (Kubin et al., 1992). The change in the x_1-position of dislocation k is $v^{(k)}\Delta t$ and annihilation of two dislocations with opposite Burgers vector occurs when they are within a material dependent, critical annihilation distance L_e, which is taken to be $L_e = 6b$.

An initial distribution of dislocation sources and obstacles is specified on each slip plane. Obstacles to dislocation motion are modeled as fixed points on a slip plane. Such obstacles account for the effects of dislocations on other, secondary, slip systems in blocking slip on the primary slip plane, or, possibly, for the effects of small precipitates. Pinned dislocations can only pass the obstacles when their Peach–Koehler force exceeds an obstacle dependent value $\tau_{obs}b$. All obstacles are taken to have the same strength $\tau_{obs} = 5.7 \times 10^{-3}\,\mu$, with μ denoting the elastic shear modulus.

No dislocations are present initially. New dislocations are generated by simulating Frank–Read sources. In two dimensions, a Frank–Read source is simulated by point sources on the slip plane which generate a dislocation dipole when the magnitude of the Peach–Koehler force at the source exceeds the critical value $\tau_{nuc}b$ during a period of time t_{nuc}. The distance L_{nuc} between the dislocations is specified as

$$L_{nuc} = \frac{\mu}{2\pi(1-\nu)}\frac{b}{\tau_{nuc}}, \tag{8}$$

where ν is Poisson's ratio. At this distance, the shear stress of one dislocation acting on the other is balanced by the slip plane shear stress. The magnitude of τ_{nuc} is randomly chosen from a Gaussian distribution with mean strength $\bar{\tau}_{nuc} = 1.9 \times 10^{-3}\,\mu$ and standard deviation $0.2\bar{\tau}_{nuc}$. With $\nu = 0.33$, this mean nucleation strength corresponds to a mean nucleation distance of $L_{nuc} = 125b$. The nucleation time for all sources is taken as $t_{nuc} = 2.6 \times 10^6 B/\mu$.

The displacement and stress fields are written as the superposition of two fields,

$$u_i = \tilde{u}_i + \hat{u}_i, \quad \sigma_{ij} = \tilde{\sigma}_{ij} + \hat{\sigma}_{ij}. \tag{9}$$

The $\tilde{}$ displacement field is the superposition of the fields of the individual dislocations in an infinite medium of the homogeneous matrix material and the $\hat{}$ fields represent the image fields that correct for the actual boundary conditions and for the presence of the particles. The $\hat{}$ fields are smooth and are solved for by the finite-element method. Both the stress–strain response and the evolution of the dislocation structure are outcomes of the boundary value solution in the discrete dislocation formulation.

2.2. Nonlocal crystal plasticity

The nonlocal continuum plasticity formulation adopted in this work is based on the simple theory proposed by Acharya and Bassani (1996, 2000) where a particular strain gradient, which is taken to be a measure of elastic (or plastic) incompatibility, enters the flow rule only through the instantaneous hardening rate. Consequently, this simple theory preserves the classical structure of incremental boundary value problems (Hill, 1958) and does not require higher-order stresses or additional boundary conditions as, for example, in the formulations in Fleck and Hutchinson (1997) and Shu and Fleck (1999).

The physical motivation for the nonlocal theory of crystal plasticity used here, which also motivated the work of Fleck et al. (1994), is based on the notion of lattice incompatibility (see Acharya and Bassani (2000) for a detailed discussion). The basic idea is that the elastic distortion of the lattice is not, in general, compatible with a regular deformation, i.e. one that is derivable from a continuously differentiable displacement field. On the other hand, that elastic distortion is capable of representing so-called

geometrically-necessary dislocations (Nye, 1953). In the formulation of Acharya and Bassani (1996, 2000), the hypothesis is that this incompatibility enters the constitutive relation only through its influence on the hardening. Since the lattice incompatibility is characterized by a gradient of the elastic (or plastic) deformation field, a material length scale enters the theory on dimensional grounds.

In the setting of small strain kinematics, the total displacement gradient is written as the sum of elastic and plastic parts:

$$u_{i,j} = u^{\mathrm{e}}_{ij} + u^{\mathrm{p}}_{ij}, \tag{10}$$

where the symmetric parts form the corresponding components of total, elastic, and plastic strains, ϵ_{ij}, $\epsilon^{\mathrm{e}}_{ij}$ and $\epsilon^{\mathrm{p}}_{ij}$, respectively. The plastic part of the displacement gradient is taken to arise solely from slips $\gamma^{(\beta)}$ on all systems $(\beta = 1, N)$ according to

$$u^{\mathrm{p}}_{ij} = \sum_{\beta} \gamma^{(\beta)} m^{(\beta)}_i n^{(\beta)}_j, \tag{11}$$

where the unit vectors $m^{(\beta)}_i$ and $n^{(\beta)}_i$, respectively, denote the slip direction and slip-plane normal for system β.

The key idea in developing the nonlocal theory is based on the observation that, even though the total displacement gradient (and total strain) is required to be compatible with a regular deformation, i.e. a continuously differentiable, single-valued displacement field, neither the elastic nor plastic parts are individually compatible in general. The significance of the incompatibility measure is seen by considering the line integral

$$w_i = \int_{x^0_j}^{x_j} v_{ij}\,\mathrm{d}y_j \tag{12}$$

with $v_{ij}(x_k)$ denoting a second-order tensor field and x^0_i an arbitrarily chosen fixed point. Application of the classical Stokes theorem for simply connected domains gives that if Eq. (12) is path independent,

$$e_{jkl} v_{il,k} = 0, \tag{13}$$

where e_{jkl} is the alternating symbol. Then, $v_{ij} = w_{i,j}$ and v_{ij} is said to be compatible with w_i. Relation (13) holds if v_{ij} is taken to be the total displacement gradient $u_{i,j}$ (Acharya and Bassani, 2000).

Accordingly, from Eqs. (13) and (11), a natural measure of incompatibility is Nye (1953) dislocation density:

$$\alpha_{ij} = e_{jkl} u^{\mathrm{p}}_{il,k} = e_{jkl} \sum_{\beta} \gamma^{(\beta)}_{,k} m^{(\beta)}_i n^{(\beta)}_l. \tag{14}$$

A nonvanishing tensor α_{ij} implies the existence of geometrically necessary dislocations. This measure can be used to compute the excess of dislocations of one sign, i.e. the net Burgers vector b_i, in any region bounded by a closed curve C:

$$b_i = \oint_C u^{\mathrm{p}}_{ij}\,\mathrm{d}x_j = \int_S e_{ljk} u^{\mathrm{p}}_{ik,j} r_l\,\mathrm{d}S, \tag{15}$$

where r_i is the unit normal to a surface S whose boundary is the curve C. Note that since $u_{i,j}$ is compatible, if u^{e}_{ij} is substituted for u^{p}_{ij}, from Eq. (10) the value of b_i will only change sign.

In the simple nonlocal crystal plasticity model used here for the continuum calculations, the measure of incompatibility is taken to influence only the instantaneous hardening rates for individual slip systems (Acharya and Bassani, 1996, 2000). The flow rule is otherwise unchanged, irrespective whether it is rate independent as in Hill (1966) or rate dependent as in the viscoplastic rule of Peirce et al. (1983) and used for the finite element calculations presented subsequently.

With $\tau_{cr}^{(\kappa)}$ taken to be the measure of hardness of slip system κ, the rate of hardening under multiple-slip deformations is given by the usual expression (Hill, 1966):

$$\dot{\tau}_{cr}^{(\kappa)} = \sum_{\beta} h_{\kappa\beta}\dot{\gamma}^{(\beta)}, \tag{16}$$

where $h_{\kappa\beta}$ denotes the instantaneous slip-system hardening matrix which, in general, depends upon the history of slip. In the nonlocal theory (Acharya and Bassani, 1996, 2000), $h_{\kappa\beta}$ is taken to depend both on the slips $\gamma^{(\kappa)}$ and on α_{ij}, the measure of incompatible lattice deformations (see also Luo, 1998).

For multiple slip deformations with $h_{\kappa\beta}(\{\gamma^{(\nu)}\}, \alpha_{ij})$, there are outstanding issues about how to apportion the effects of incompatibility on each slip system or, more precisely, to each component of $h_{\kappa\beta}$. Given that the present study only involves single slip and two-dimensional deformation, the remaining discussion of hardening will be limited to when those two conditions hold. In this case, it is immediately clear that the gradient of slip in the direction normal to a slip plane, $\gamma_{,k}n_k$, does not contribute to the right-hand side of Eq. (14). Therefore, for single slip in two dimensions with $\gamma(x_1, x_2)$ and $\mathbf{m} = \mathbf{e}_1$, the only nonzero component of α_{ij} is

$$\alpha_{13} = \gamma_{,1}. \tag{17}$$

Hence, in this case, with $\dot{\tau}_{cr} = h\dot{\gamma}$ and incorporating the effect of incompatibility, the slip-system hardening-rate, $h = \mathrm{d}\tau/\mathrm{d}\gamma$, is taken to depend only on γ and $\gamma_{,1}$.

Consistent with the experimentally verified notion that hardening is increased in the presence of gradients associated with incompatibility, in single slip a simple modification of the slip system strain hardening rule used in Cleveringa et al. (1997) is adopted:

$$h(\gamma, \gamma_{,1}) = h_0\left(\frac{\gamma}{\gamma_0} - 1\right)^{N-1}\left[1 + \ell^2\left(\frac{\gamma_{,1}}{\gamma_0}\right)^2\right]^{\mathrm{p}}, \tag{18}$$

where ℓ is the intrinsic length scale (which is typically on the order of microns) and p is a parameter, which is typically positive and less than unity. A similar hardening function with $\gamma_{,1}$ replaced by the appropriate measures of incompatibility has been used by Luo (1998) in studies of torsion and biaxial stretching of films for isotropic materials.

The viscoplastic flow rule for single slip, which is used in the finite element calculations presented below, is taken to be a power law:

$$\dot{\gamma} = \dot{\gamma}_0\left(\frac{\tau}{\tau_{cr}}\right)\left(\left|\frac{\tau}{\tau_{cr}}\right|\right)^{1/m-1}, \tag{19}$$

where $\dot{\gamma}_0$ is a reference strain rate, m is the strain-rate hardening exponent, τ_{cr} is the slip system hardness, and $\tau = \sigma_{12}$ is the slip-system resolved shear stress.

Using

$$\dot{\epsilon}_{ij}^{\mathrm{e}} = \mathscr{L}_{ijkl}^{-1}\dot{\sigma}_{kl} \tag{20}$$

together with the rate form of Eqs. (10) and (11), restricting the attention to single slip, and inverting gives

$$\dot{\sigma}_{ij} = \mathscr{L}_{ijkl}\left[\dot{\epsilon}_{kl} - \frac{\dot{\gamma}}{2}(m_k n_l + m_l n_k)\right] \tag{21}$$

with $\dot{\gamma}$ given by Eq. (19). The constitutive equation (21) has the same form as in a local theory, but with the nonlocal (gradient) effect entering the expression (19) for $\dot{\gamma}$ through τ_{cr} which evolves through a dependence on both γ and $\gamma_{,1}$ via Eqs. (16) and (18).

Relation (21) is substituted into Eq. (1), and this forms the basis for the finite-element discretization. In order to increase the stable time step, the forward gradient method of Peirce et al. (1983) is used. Calculation of the gradient $\gamma_{,1}$ for use in the hardening expression (18) is the only change required in a computer program for the usual local crystal plasticity formulation. In this paper, the discretization is based on rectangular elements consisting of four "crossed" linear displacement triangles. The values of γ are stored at the centroids of each triangular element. The gradient $\gamma_{,1}$ is computed in the following fashion: first, for each rectangle, the values of γ are extrapolated from the four triangle centroids to the nodal points of the rectangular element using bilinear shape functions. Then, the value of γ associated with a node is taken to be the average value of each rectangle connected to that node. With the rectangular element defined by $x_- \leqslant x \leqslant x_+$ and $y_- \leqslant y \leqslant y_+$, we set $\gamma_{,1} = (\gamma_+ - \gamma_-)/(x_+ - x_-)$, where γ_+ is the average of the two nodes having x-coordinate x_+ and γ_- is the average of the two nodes having x-coordinate x_-. The value of $\gamma_{,1}$ is taken to be the same for each triangle making up the rectangle.

3. Comparison of discrete dislocation and nonlocal continuum plasticity predictions

The two-dimensional, discrete dislocation simulations of Cleveringa et al. (1997, 1998) are regarded as numerical experiments for the behavior of rectangular elastic particles embedded in a plastically deforming, single crystal matrix. Complete details of the parameters entering the calculations, as well as further references, are given in Cleveringa et al. (1997, 1998). It suffices to give a brief summary of the key results, before discussing the fit of these results with the nonlocal continuum model.

3.1. Discrete dislocation simulations

Curves of average shear stress, defined in Eq. (5), versus imposed shear strain Γ from the discrete dislocation simulations in Cleveringa et al. (1997) are shown in Fig. 2 for the two composite morphologies, material (i) and (iii), with a cell size $c = L = 1$ μm. There is essentially no overall hardening for material (i), and in fact there is some degree of softening accompanying the strain localization. In contrast, material (iii) displays significant hardening and, as shown in Fig. 3 for $c = 0.5, 1$ and 2 μm (taken from Cleveringa et al.,

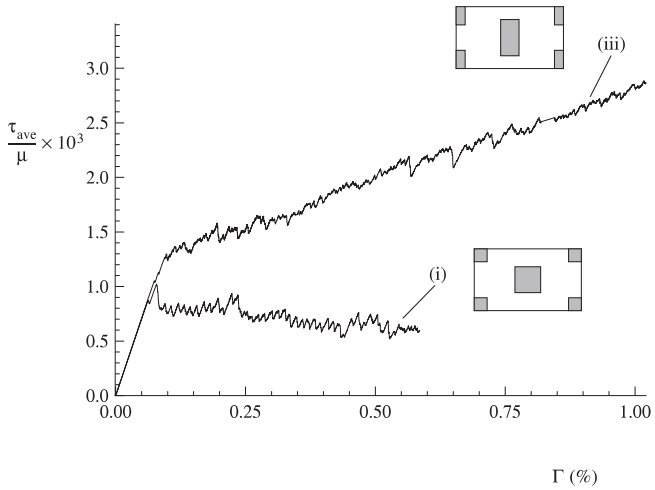

Fig. 2. Effect of morphology on the discrete dislocation predictions for the overall shear-stress response.

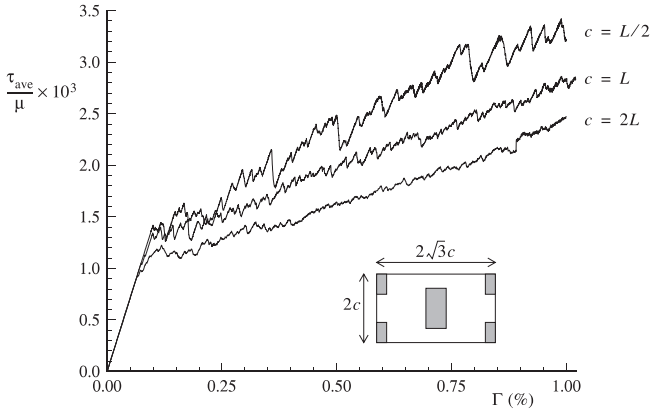

Fig. 3. Shear-stress response to simple shear of composite materials with various size scales of particles.

1998), also displays significant cell size dependence. Furthermore, Cleveringa et al. (1997) demonstrated that these differences cannot be captured by a local continuum model with the same single-crystal matrix material for both composite morphologies. For the cell size they investigated, the level of matrix hardening required in a purely local model to reproduce the dislocation results for material (iii) is significantly higher than the hardening required for material (i).

The overall behavior of material (i) is, in fact, close to that of the matrix material itself since there are unblocked channels of slip for that composite morphology with $c = 1$ μm as seen in the dislocation distribution of Fig. 4a at $\Gamma = 0.58$ (from Cleveringa et al., 1997). Such a region of localized dislocation activity is termed coarse slip. Other recent calculations for material (i) (not reproduced here for brevity) also display little dependence on the absolute cell size, at least for cell sizes that are large compared to the spacing of the slip planes which is taken to be 100 Burgers vectors or 25 nm in those calculations.

Material (iii) is significantly harder because every path of slip across the cell (lines parallel to the x_1-direction) is blocked by a particle as seen in Fig. 4b, which is the dislocation distribution at $\Gamma = 0.01$ with $c = 1$ μm (from Cleveringa et al., 1997). This difference in slip distribution has an important implication with respect to lattice incompatibility or, equivalently, geometrically necessary dislocations. As discussed with reference to Eq. (17), slip gradients in the direction normal to the slip plane, which are certainly high in the neighborhood of the coarse slip bands of material (i), do not cause incompatibility. Blocked slip, in contrast, not only impedes coarse slip, but it also enhances gradients in the slip plane (in the x_1-direction). Therefore, blocked slip also enhances lattice incompatibility, in particular, through $\gamma_{,1}$ which is the only contribution to Nye's dislocation density tensor here.

3.2. Nonlocal crystal plasticity results

The discrete dislocation simulations are compared with the predictions of the nonlocal plasticity theory. The matrix parameters entering Eqs. (18) and (19) are taken to be $\tau_0/\mu = 1.33 \times 10^{-3}$, $h_0/\mu = 2.47 \times 10^{-3}$ or 2.47×10^{-4}, $\gamma_0 = 0.002$, $N = 1$ or 0.3, $\ell = 1, 5, 10$ or 20 μm, $p = 0.5$ and strain-rate sensitivity parameters $\dot{\gamma}_0 = 0.002\ \mathrm{s}^{-1}$ and $m = 0.005$.

The single-crystal matrix parameters entering the nonlocal continuum model were chosen in an attempt to give composite shear stress versus shear strain curves similar to the discrete dislocation simulations for both composite morphologies at a size scale of $c = 1$ μm. The process of selecting matrix properties in Eq. (18) is based on a few observations, the first two of which concern parameters that enter the local part of the matrix description: (a) h_0 should be low enough to give minimal hardening for material (i); (b) at that fairly

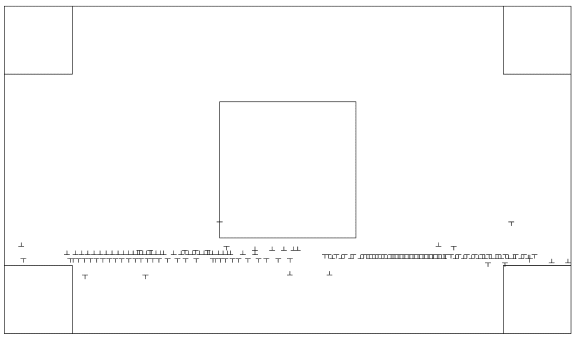

(a)

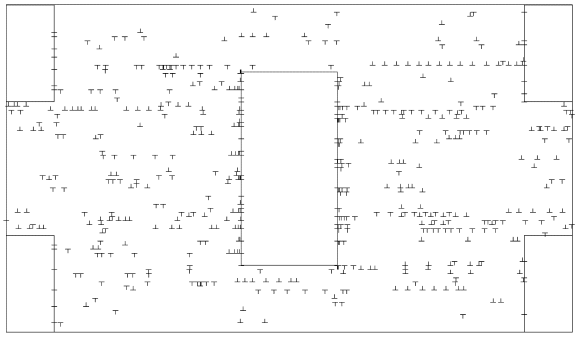

(b)

Fig. 4. Predicted dislocation distributions in (a) material (i) and (b) material (iii).

low value of h_0 and for an overall shear strain $\Gamma \leqslant 0.01$ (as in the discrete dislocation calculations), the effect of the power-law exponent N was not expected to be too significant; and (c) the effect of incompatibility on hardening as measured in two-dimensional single slip in terms of $\gamma_{,1}$ in Eq. (18) depends strongly on the nonlocal parameters ℓ and p. The effects of cell size are explored by varying the nondimensional ratio c/ℓ with all other material parameters held fixed ($p = 0.5$).

Numerical results for the average shear stress τ_{ave} versus applied shear strain Γ are plotted in Figs. 5–8 for the two composite morphologies and various material parameters and cell sizes, c, normalized by the material length scale ℓ, where $c/\ell \to \infty$ corresponds to purely local behavior ($\ell = 0$). Unless specified otherwise, a mesh consisting of 680 quadrilateral elements was used for the calculations. From comparisons of these plots with the discrete dislocation results for the overall behavior, a set of matrix material parameters can be chosen that give reasonable agreement with the results of the discreet dislocation simulations. For brevity, only results for two nominal hardening rates, h_0/μ, and two power-law exponents, N, are presented that together roughly bracket the discrete dislocation results. The first of these results are for material (iii). Fig. 5a and b are τ_{ave} versus Γ curves for $N = 1$ and for $h_0/\mu = 2.47 \times 10^{-4}$ and $h_0/\mu = 2.47 \times 10^{-3}$, respectively, at various normalized cell sizes c/ℓ. The corresponding results for $N = 0.3$ are plotted in Fig. 6a and b.

The purely local results, $c/\ell \to \infty$, for material (iii) plotted in Figs. 5–8 display quite similar trends for both levels of matrix hardening and for both hardening exponents. In particular, comparing Fig. 5a and b shows that at $\Gamma = 0.01$, the shear stress given by the local theory with $N = 1$ and with $h_0/\mu = 2.47 \times 10^{-3}$ is

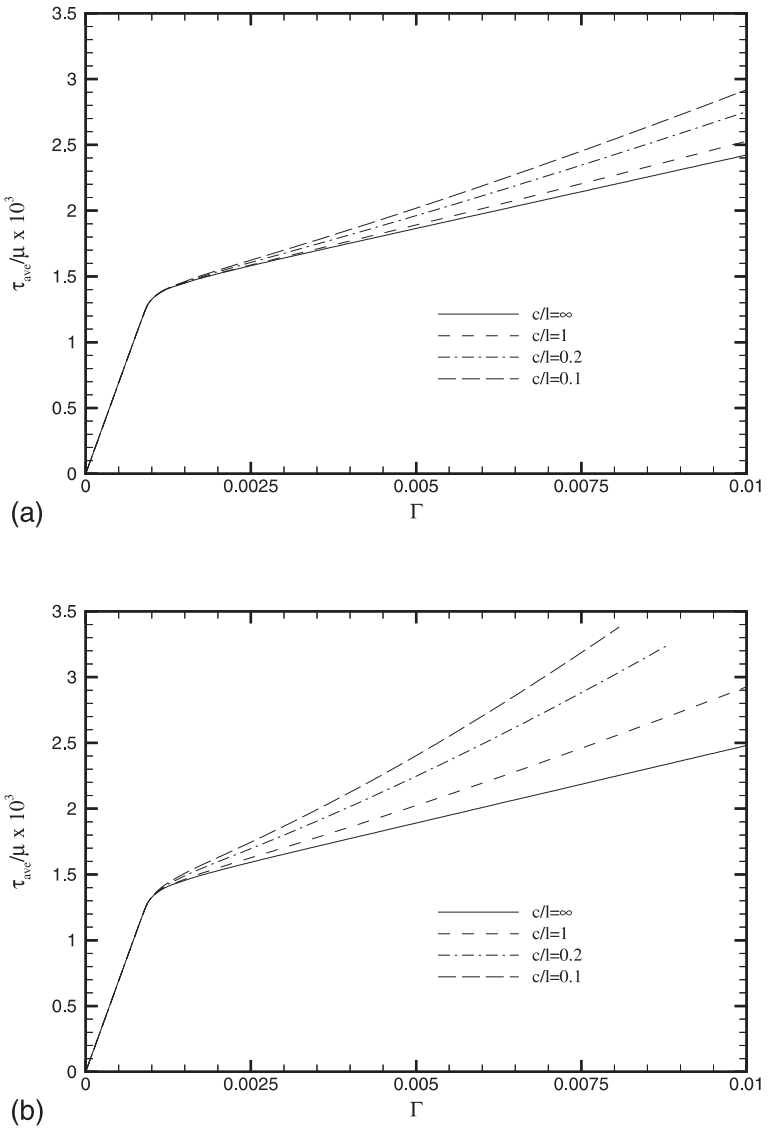

Fig. 5. Average shear stress τ_{ave} versus applied shear strain Γ for material (iii) according to the nonlocal continuum plasticity model with $N = 1$ and (a) the lower matrix hardening rate, $h_0/\mu = 2.47 \times 10^{-4}$ and (b) the higher matrix hardening rate, $h_0/\mu = 2.47 \times 10^{-3}$, and for various ratios of cell sizes to material length scale ($c/\ell \to \infty$ corresponds to purely local behavior).

only a few percent higher than for the corresponding calculation with $h_0/\mu = 2.47 \times 10^{-4}$; the difference in stress level for the two local theory calculations in Fig. 6, where $N = 0.3$, is even smaller.

On the other hand, with nonlocal hardening behavior and c/ℓ on the order of 0.1 to 1, there is considerably more overall hardening and greater size-scale effects for the higher value of h_0 (Figs. 5b and 6b) as well as for the higher value of N (Fig. 5a and b). This effect of h_0 and N on nonlocal behavior is a consequence of the assumed multiplicative influence of incompatibility on hardening as prescribed in Eq. (18). (For an additive contribution to the hardening rate from incompatibility, which is also plausible, the parameters entering the purely local contribution would be expected to have less effect on nonlocal behavior.)

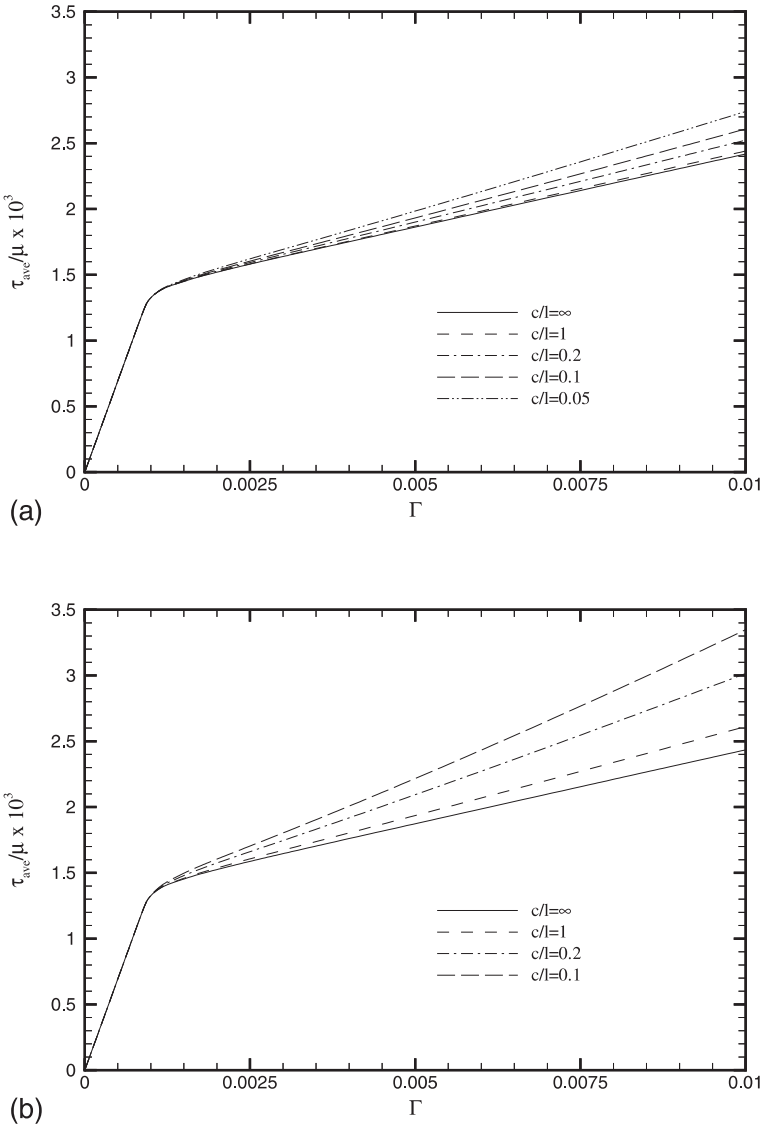

Fig. 6. Average shear stress τ_{ave} versus applied shear strain Γ for material (iii) according to the nonlocal continuum plasticity model with $N = 0.3$ and (a) the lower matrix hardening rate, $h_0/\mu = 2.47 \times 10^{-4}$ and (b) the higher matrix hardening rate, $h_0/\mu = 2.47 \times 10^{-3}$, and for various ratios of cell sizes to material length scale ($c/\ell \to \infty$ corresponds to purely local behavior).

Furthermore, with $p \geqslant 0$, this nonlocal factor leads to a slight upturn in the overall τ_{ave} versus Γ curves, since the term in square brackets in Eq. (18) increases with increasing $\gamma_{,1}$ as γ itself increases. This effect is most clearly seen for $N = 1$; for $N = 0.3$ the effect is reduced by the softening in the local term in Eq. (18). A smaller value of p would also lessen the upturn.

The tendency for the upturn in the overall τ_{ave} versus Γ curves at larger strains, particularly for $N = 1$, can be offset with a simple modification to the way in which the slip gradient enters the hardening rate. One such modification that was adopted by Luo (1998) in studies of torsion of thin wires and biaxial stretching of thin films replaces the term $\left(\gamma_{,1}/\gamma_0\right)^2$ in Eq. (18) by $\gamma_{,1}^2/\left(\gamma^2 + \gamma_0^2\right)$ which reduces the gradient-hardening

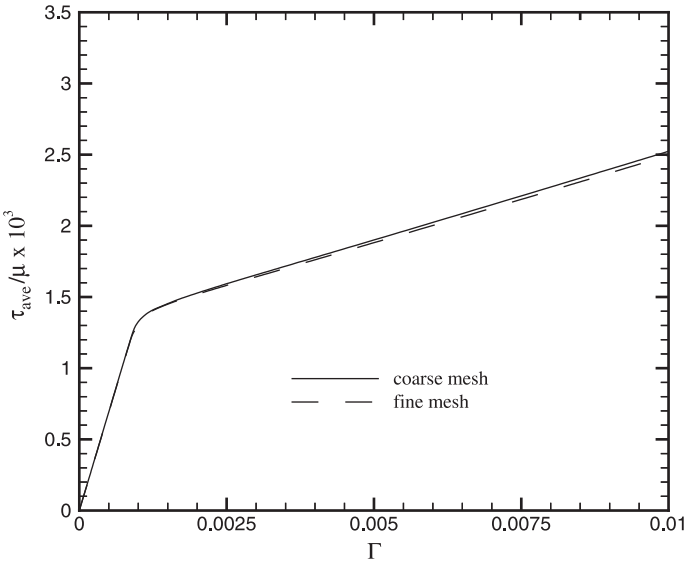

Fig. 7. Comparison of coarse and fine mesh solutions: average shear stress τ_{ave} versus applied shear strain Γ for material (iii) with $N = 0.3$, the lower matrix hardening rate, $h_0/\mu = 2.47 \times 10^{-4}$, and $c/\ell = 0.2$.

effect at larger strains and, depending on the magnitude of γ_0, can increase the gradient effects at smaller strains.

A finer mesh consisting of 6120 elements was used to study the accuracy of the solutions utilizing 680 elements as in Figs. 5 and 6. Fig. 7 shows that there is little difference in the composite stress–strain response predicted by the two meshes for material (iii) with $N = 0.3$, $h_0/\mu = 2.47 \times 10^{-4}$, and $c/\ell = 0.2$. In general, there is good agreement between predictions based on the two mesh resolutions. It is worth noting that the convergence was generally better for smaller values of c/ℓ because one effect of nonlocality is to smooth out gradients.

For material (i) in the range $\Gamma \leqslant 0.01$, we found even less dependence on N, compared to material (iii), given the low level of overall hardening predicted by the discrete dislocation simulations. Consequently, for brevity only the τ_{ave} versus Γ results for $N = 0.3$ are presented in Fig. 8a and b for $h_0/\mu = 2.47 \times 10^{-4}$ and $h_0/\mu = 2.47 \times 10^{-3}$, respectively. For both hardening levels, the curves for the homogeneous matrix material are indistinguishable from the local results ($c/\ell \to \infty$) for material (i). With effects of incompatibility on hardening included for the range of c/ℓ considered, the initial matrix hardening rate $h_0/\mu = 2.47 \times 10^{-4}$ gives overall hardening for material (i), which is only slightly higher than that for the pure matrix, whereas $h_0/\mu = 2.47 \times 10^{-3}$ leads to considerably higher hardening at the smaller size scales (smaller values of c/ℓ), which is not consistent with the discrete dislocation results. The lower matrix hardening rate, $h_0/\mu = 2.47 \times 10^{-4}$, leads to trends that are more in accord with the discrete dislocation predictions.

From Figs. 5 and 6 for material (iii), we note that the average stress at $\Gamma = 0.01$ with purely local matrix behavior ($c/\ell \to \infty$) is about $\tau_{ave}/\mu = 2.4 \times 10^{-3}$, while the corresponding discrete dislocation result from Fig. 6 predicts $\tau_{ave}/\mu = 2.8 \times 10^{-3}$, which is about 17% higher. At the lower level of hardening ($h_0/\mu = 2.47 \times 10^{-4}$), for $N = 1$ (Fig. 5a) this difference is made up by the nonlocal material with $c/\ell = 0.2$ ($\ell = 5\mu m$); for $N = 0.3$ (Fig. 6a), $c/\ell = 0.05$ ($\ell = 20$ μm) raises the average stress to about the same level. Of course, if only the behavior of material (iii) is to be reproduced by the continuum model, one could choose other combinations of h_0, N, and ℓ that qualitatively agree with the discrete dislocation results of Fig. 2 for $c = 1$ μm. On the other hand, if the behavior of material (i), which displays little effect of the reinforcement on the composite stress–strain response, is also to be accurately modeled, then a relatively low value of h_0 is

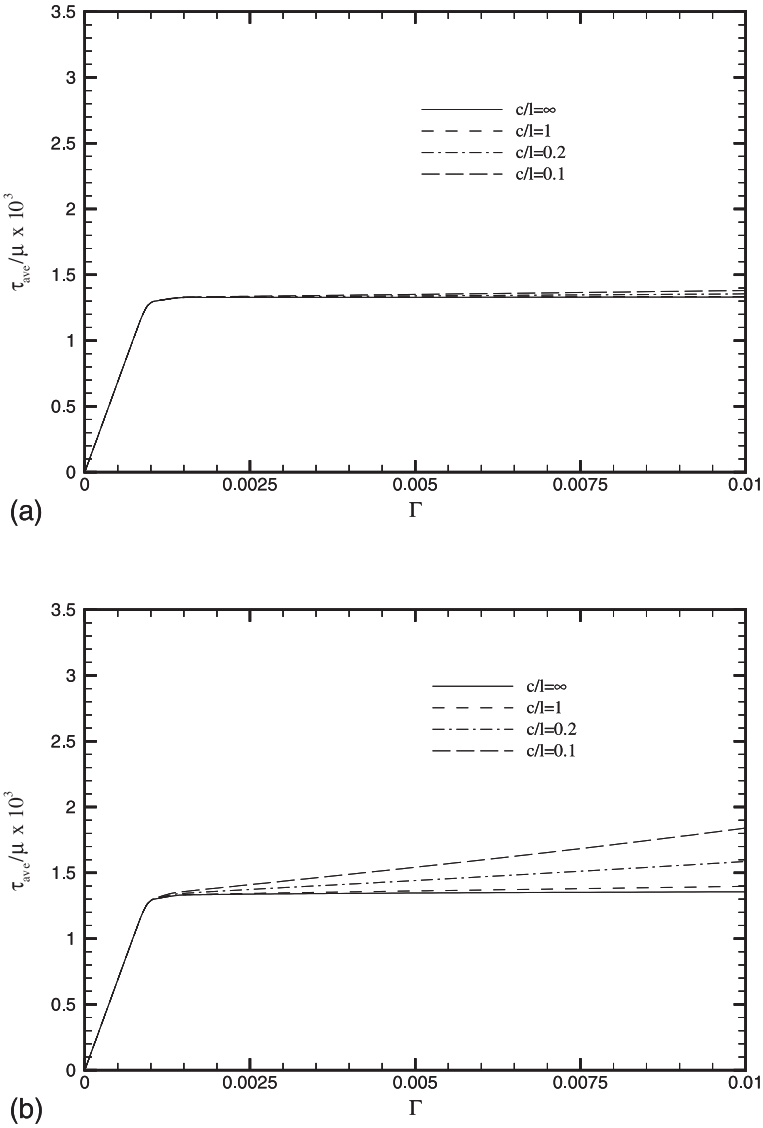

Fig. 8. Average shear stress τ_{ave} versus applied shear strain Γ for material (i) according to the nonlocal continuum plasticity model with $N = 0.3$ and (a) the lower matrix hardening rate, $h_0/\mu = 2.47 \times 10^{-4}$ and (b) the higher matrix hardening rate, $h_0/\mu = 2.47 \times 10^{-3}$, and for various ratios of cell sizes to material length scale ($c/\ell \to \infty$ corresponds to purely local behavior).

required. Therefore, either of the two aforementioned sets of parameters N and ℓ at the lower hardening level ($h_0/\mu = 2.47 \times 10^{-4}$) can reasonably reproduce the trends of both material (i) and material (iii) for $c = 1$ μm. Again we note that the parameter set which includes $N = 0.3$ displays less tendency for an upturn in the τ_{ave} versus Γ curves.

One can see from Figs. 5 and 6, that as the cell size for material (iii) decreases with the area fraction of inclusions kept fixed, i.e. as c/ℓ decreases, that the overall hardening rate tends to increase. This is also seen in the discrete dislocation results of Fig. 3. Cleveringa et al. (1998) considered a power-law fit to results like those in Fig. 3:

$$\frac{d\tau_{ave}}{d\Gamma} \propto c^{-\beta}. \tag{22}$$

From over 10 simulations for different cell sizes and for different initial densities and distributions of dislocation sources and obstacles, they found that at an overall shear strain of $\Gamma = 0.01$, the best fit gives $\beta \approx 1/3$. In the continuum model, this relationship depends both on N and h_0/μ. For $N = 0.3$, from the finite element results of Fig. 6 at $\Gamma = 0.01$, $\beta \approx 0.3$ for $h_0/\mu = 2.47 \times 10^{-3}$ and $\beta \approx 0.2$ for $h_0/\mu = 2.47 \times 10^{-4}$.

Next, contours of the strain and strain-gradient fields are presented to provide a better understanding of the effects of nonlocal hardening. For material (iii), contours of plastic slip, $\gamma = \int \dot{\gamma}\, dt$, where $\dot{\gamma}$ is given by Eq. (19), for $N = 1$, $h_0/\mu = 2.47 \times 10^{-4}$ are plotted in Fig. 9 for overall shear strain $\Gamma = 0.01$; Fig. 9a is the nonlocal result with $c/\ell = 0.2$ and Fig. 9b is the local result ($c/\ell \to \infty$). The corresponding contours of the plastic slip gradient $\gamma_{,1}$ are plotted in Fig. 10a and b. In general, the effects of nonlocal hardening associated with incompatible lattice deformations cause a reduction in the gradient $\gamma_{,1}$ which, in this two-dimensional, single-slip problem, is the unique measure of incompatibility. In other words, the resulting slip (plastic strain) fields for the nonlocal model tend to be smoother than for the purely local behavior.

Similar contour plots for material (i) are presented in Figs. 11 and 12 for the same set of material parameters and for $c/\ell = 0.2$. Since $\gamma_{,2}$ is the only significant gradient of slip arising in that composite morphology, which neither gives rise to incompatibility nor, therefore, to gradient hardening, there is little difference between the local and nonlocal fields. The coarse slip band which develops in the continuous channel of matrix material is clearly seen in Fig. 11.

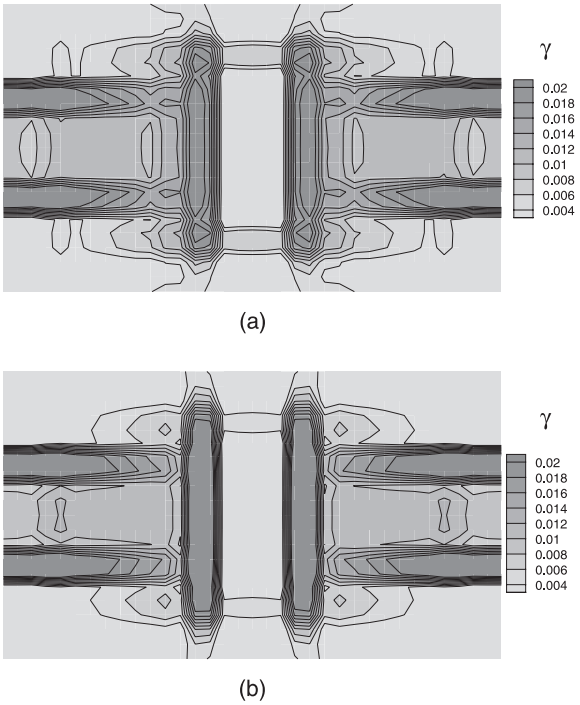

Fig. 9. Contours of slip γ for material (iii) with $N = 1$ and the lower matrix hardening rate, $h_0/\mu = 2.47 \times 10^{-4}$, at $\Gamma = 0.01$: (a) $c/\ell = 0.2$ and (b) $c/\ell \to \infty$ corresponding to purely local behavior.

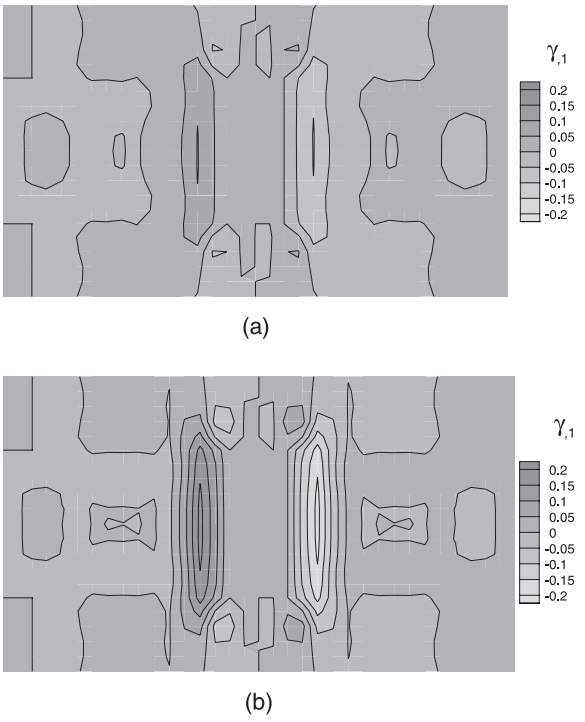

Fig. 10. Contours of slip gradient $\gamma_{,1}$ for material (iii) with $N = 1$ and the lower matrix hardening rate, $h_0/\mu = 2.47 \times 10^{-4}$, at $\Gamma = 0.01$: (a) $c/\ell = 0.2$ and (b) $c/\ell \to \infty$ corresponding to purely local behavior.

Cleveringa et al. (1997) observed that discrete dislocation plasticity gave rise to a greater proportion of the shear stress being carried by the reinforcement than predicted by local, size-independent plasticity theory. To check the predictions of the nonlocal theory, we have computed phase averages of the shear stress for material (iii) at $\Gamma \approx 0.01$ with $h_0/\mu = 2.47 \times 10^{-4}$ and $N = 1$. The proportion of the stress carried by the reinforcement decreases as c/ℓ increases; $\langle\sigma_{12}\rangle_r/\tau_{\text{ave}} = 3.21$, 3.20, 3.08 and 3.00 for $c/\ell = 0.1$, 0.2, 1.0 and ∞ (the local theory), respectively, where $\langle\sigma_{12}\rangle_r$ is the average shear stress in the reinforcement phase. With $h_0/\mu = 2.47 \times 10^{-4}$, $N = 0.3$ and $c/\ell = 0.05$, $\langle\sigma_{12}\rangle_r/\tau_{\text{ave}} = 2.96$ at $\Gamma = 0.01$. The discrete dislocation results in Cleveringa et al. (1997) have $\langle\sigma_{12}\rangle_r/\tau_{\text{ave}} = 3.06$ at $\Gamma = 0.0058$, whereas their local continuum slip calculation, which requires a much higher matrix hardening of $h_0/\mu = 4.94 \times 10^{-3}$ in order to match the composite stress–strain behavior with the local theory, only gives $\langle\sigma_{12}\rangle_r/\tau_{\text{ave}} = 2.36$. In contrast, the nonlocal theory used here, with a lightly hardening matrix, gives a good agreement with the composite phase average shear-stress distribution. Comparison of the phase average shear stresses provides a basis for identifying material parameters that supplements the comparison of overall stress–strain behavior. However, in addition, the discrete dislocation results show local stress concentrations in the reinforcement that arise from dislocations piled up against the reinforcement sides. These local stress concentrations do not occur in the nonlocal plasticity calculations, although the elevation in the average stress in the reinforcement is reasonably well reproduced.

Finally, it is interesting to consider the nonlocal response when the full gradient of slip, rather than the incompatibility measure, raises the level of hardening. As a simple example for comparison purposes, consider the term $\sqrt{\gamma_{,1}^2 + \gamma_{,2}^2}$ in place of $\gamma_{,1}$ in Eq. (18) and otherwise the same description of the matrix material as defined in Section 2.2. With $h_0/\mu = 2.47 \times 10^{-4}$, for $N = 0.3$, and $c/\ell = 0.2$, the effect of $\gamma_{,2}$ is

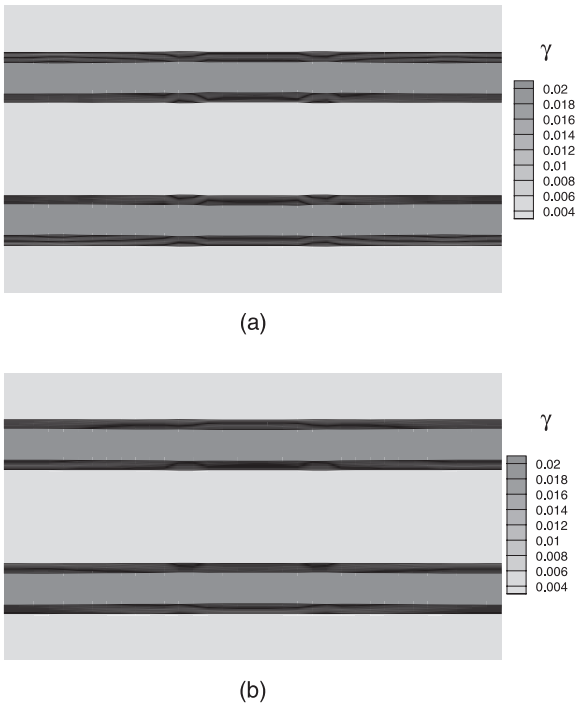

Fig. 11. Contours of slip γ for material (i) with $N = 1$ and the lower matrix hardening rate, $h_0/\mu = 2.47 \times 10^{-4}$, at $\Gamma = 0.01$: (a) $c/\ell = 0.2$ and (b) $c/\ell \to \infty$ corresponding to purely local behavior.

significant for material (i), whereas it is relatively small for material (iii), as seen in Fig. 13. Since there is little effect of the addition of $\gamma_{,2}$ to the hardening for material (iii), the corresponding slip and slip-gradient contours are similar to those in Figs. 9a and 10a. On the other hand, for material (i) there are significant differences. Fig. 14 is a contour plot of γ, where Fig. 14a corresponds to the physically-based hardening model (18), and Fig. 14b corresponds to the a hardening model with $\sqrt{\gamma_{,1}^2 + \gamma_{,2}^2}$ replacing $\gamma_{,1}$ in Eq. (18). Clearly, whereas the nonlocal hardening model, which uses the gradient associated with incompatibility, reasonably distinguishes between materials (i) and (iii), the model incorporating the full gradient does not.

4. Concluding remarks

Predictions of the nonlocal plasticity theory of Acharya and Bassani (1996, 2000) for the response of a model composite material have been compared with the results of discrete dislocation simulations. Two composite morphologies have been considered: for one, the discrete dislocation simulations exhibit significant strain hardening, with the overall stress–strain response being strongly size-dependent; for the other, which has a channel of material that allows slip to propagate relatively unimpeded across the cell, the discrete dislocation response is approximately ideally plastic (slightly softening), with no significant size dependence. Material parameters are found for which the nonlocal plasticity calculations are in reasonable agreement with the discrete dislocation predictions. It is worth emphasizing that the plastic flow properties of the nonlocal theory are fit to the discrete dislocation results for one composite morphology and size; the nonlocal theory then predicts the dependence of the response on morphology and size.

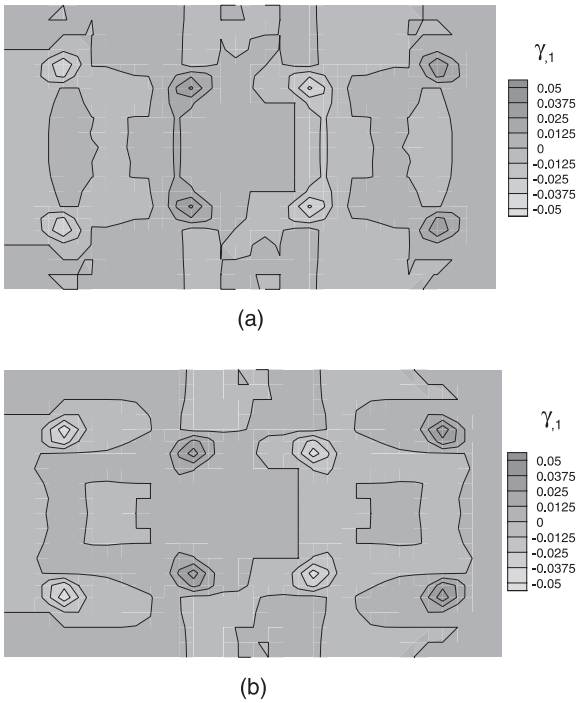

Fig. 12. Contours of slip gradient $\gamma_{,1}$ for material (i) with $N = 1$ and the lower matrix hardening rate, $h_0/\mu = 2.47 \times 10^{-4}$, at $\Gamma = 0.01$: (a) $c/\ell = 0.2$ and (b) $c/\ell \to \infty$ corresponding to purely local behavior.

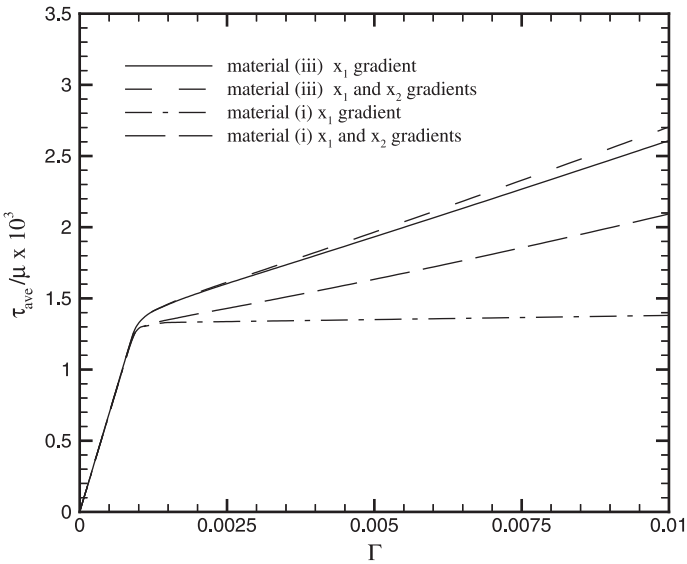

Fig. 13. Comparison of average shear stress τ_{ave} versus applied shear strain Γ for cases where the gradient hardening depends only on $\gamma_{,1}$ with cases where the hardening depends on $\gamma_{,1}$ and $\gamma_{,2}$, both with $N = 0.3$, and the lower matrix hardening rate, $h_0/\mu = 2.47 \times 10^{-4}$ for materials (i) and (iii).

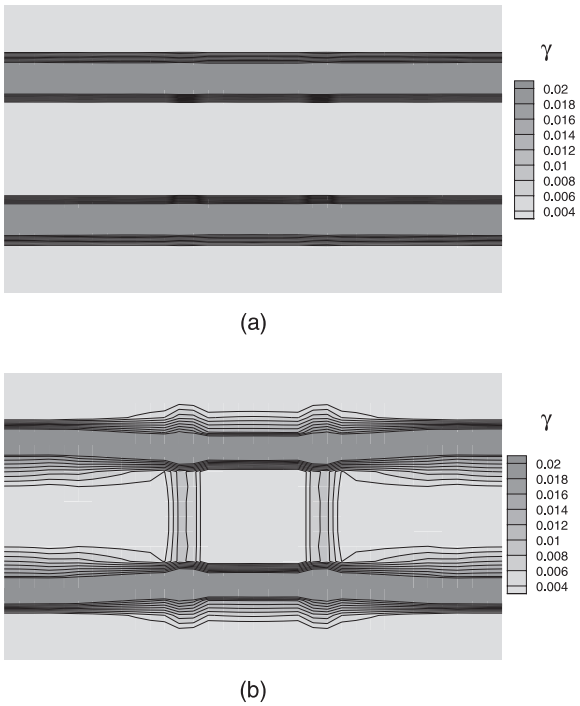

Fig. 14. Contours of slip γ for material (i) with $N = 0.3$ and the lower matrix hardening rate, $h_0/\mu = 2.47 \times 10^{-4}$, at $\Gamma = 0.01$: (a) hardening a function of $\gamma_{,1}$ only and (b) hardening a function of $\gamma_{,1}$ and $\gamma_{,2}$.

For the two-dimensional, single-slip problem considered here, the implication of incompatible lattice deformations in the nonlocal plasticity theory is particularly straightforward. The relevant measure is the gradient of slip in the direction along the slip plane, i.e. in the direction of slip itself. Gradients of slip normal to the slip plane do not give rise to incompatible lattice deformations. Consequently, the response depends sensitively on whether the particular composite morphology leads to slip patterns that involve such gradients. A local theory (Cleveringa et al., 1997) or a model incorporating the full gradient does not predict the dependence of the composite behavior on the reinforcement morphology seen in the discrete dislocation simulations.

The comparisons here have shown that, with appropriately chosen material parameters, the simple nonlocal theory of Acharya and Bassani (1996, 2000) can reproduce several trends seen in the discrete dislocation simulations of Cleveringa et al. (1997, 1998). The structure of the boundary value problems within this theory is the same as for conventional size independent plasticity theories. Hence, it is easy to implement in a standard finite element code. Furthermore, on computers of similar speed, the computing time for the nonlocal plasticity calculations is a few minutes, while it is many hours for the discrete dislocation simulations in Cleveringa et al. (1997). In particular, the time steps that can be taken in the nonlocal theory are, for a given time integration algorithm, essentially the same as for the conventional plasticity theory whereas much smaller time steps are required for the discrete dislocation simulations. Thus, the computational advantage of nonlocal plasticity theory will increase for lower strain rates and larger strains.

Many issues remain in the development of an appropriate framework for a nonlocal theory of size dependent plasticity. For example, in the theory of Acharya and Bassani (1996, 2000), under multiple slip, the issue of how to apportion lattice incompatibility to individual slip systems is unresolved. For the

theories involving higher-order stresses as in Fleck and Hutchinson (1997) and Shu and Fleck (1999), there is the issue of appropriately specifying higher order boundary conditions. Gurtin's (2000) theory has similar issues. In addition, subgrain dislocation structures are observed, e.g. in Hughes and Hansen (1993), that emerge under nominally uniform macroscopic deformations. Ortiz et al. (1999) have formulated a theory that is quite different from the nonlocal plasticity theories of Acharya and Bassani (1996, 2000), Arsenlis and Parks (1999), Fleck and Hutchinson (1997), Shu and Fleck (1999) and Gurtin's (2000), but that also gives rise to increasing strength with decreasing size. There is, as yet, no unified nonlocal plasticity framework for describing both the effects of subgrain dislocation structures that can emerge under nominally uniform deformations and the effects of geometrically necessary dislocations that are associated with strain gradients.

Acknowledgements

J.L.B. is pleased to acknowledge the hospitality of the Division of Engineering, Brown University during a sabbatical leave in 1997. A.N. is grateful for support from the Materials Research Science and Engineering Center on On Micro- and Nano-Mechanics of Materials at Brown University (NSF Grant DMR-9632524).

References

Acharya, A., Bassani, J.L., 1996. On non-local flow theories that preserve the classical structure of incremental boundary value problems. In: Pineau, A., Zaoui, A. (Eds.), Proceedings of the IUTAM Symposium on Micromechanics of Plasticity and Damage of Multiphase Materials. Kluwer Academic Publishers, Dordrecht, pp. 3–10.

Acharya, A., Bassani, J.L., 2000. Lattice incompatibility and a gradient theory of crystal plasticity. J. Mech. Phys. Solids 48, 1565–1595.

Arsenlis, A., Parks, D.M., 1999. Crystallographic aspects of geometrically-necessary and statistically stored dislocation density. Acta Mat. 47, 1597–1611.

Bilby, B.A., Bullough, R., Smith, E., 1955. Continuous distributions of dislocations: a new application of the methods of non-Riemannian geometry. Proc. Roy. Soc. London A 231, 263–273.

Brown, L.M., Ham, R.K., 1971. Dislocation-particle interactions. in: Strengthening Methods in Crystals, Elsevier, Amsterdam, pp. 12–135.

Cleveringa, H.H.M., Van der Giessen, E., Needleman, A., 1997. Comparison of discrete dislocation and continuum plasticity predictions for a composite material. Acta Mater. 45, 3163–3179.

Cleveringa, H.H.M., Van der Giessen, E., Needleman, A., 1998. Discrete dislocation simulations and size dependent hardening in single slip. J. Physique IV, 83–92.

Cleveringa, H.H.M., Van der Giessen, E., Needleman, A., 1999. A discrete dislocation analysis of bending. Int. J. Plast. 15, 837–868.

DeGuzman, M.S., Neubauer, G., Flinn, P., Nix, W.D., 1993. The role of indentation depth on the measured hardness of materials. Mater. Res. Symp. Proc. 308, 613–618.

Ebeling, R., Ashby, M.F., 1966. Dispersion hardening of copper single crystals. Phil. Mag. 13, 805–834.

Fleck, N.A., Hutchinson, J.W., 1993. A phenomenological theory for strain gradient effects in plasticity. J. Mech. Phys. Solids 41, 1825–1857.

Fleck, N.A., Hutchinson, J.W., 1997. Strain gradient plasticity. Adv. Appl. Mech. 33, 295–361.

Fleck, N.A., Muller, G.M., Ashby, F., Hutchinson, J.W., 1994. Strain gradient plasticity: theory and experiment. Acta Metall. Mater. 42, 475–487.

Gurtin, M., 2000. On plasticity of crystals: free energy, microforces, plastic strain gradients, J. Mech. Phys. Solids 48, 989–1036.

Hill, R., 1958. A general theory of uniqueness and stability in elastic-plastic solids. J. Mech. Phys. Solids 6, 236–249.

Hill, R., 1966. Generalized constitutive relations for incremental deformation of metal crystals by multislip. J. Mech. Phys. Solids 14, 95–102.

Hirth, J.P., Lothe, J., 1968. Theory of Dislocations. McGraw Hill, New York.

Hughes, D.A., Hansen, N., 1993. Microstructural evolution in nickel during rolling from intermediate to large strains. Metall. Trans. A 24, 2021–2037.

Kröner, E., Seeger, A., 1959. Nicht-lineare elastizitätstheorie der versetzungen und eigenspannungen. Arch. Rat. Mech. Analys. 3, 97–119.

Kubin, L.P., Canova, G., Condat, M., Devincre, B., Pontikis, V., Bréchet, Y., 1992. Dislocations microstructures and plastic flow: 3D simulation. Solid State Phenom. 23, 24, 455–472.

Luo, M., 1998. Incompatibility theory of nonlocal plasticity and applications. Ph.D. Thesis, University of Pennsylvania.

Ma, Q., Clarke, D.R., 1995. Size dependent hardness of silver single crystals. J. Mater. Res. 10, 853–863.

Nabarro, F.R.N., 1967. Theory of Crystal Dislocations. Oxford University Press, Oxford.

Nan, C.-W., Clarke, D.R., 1996. The influence of particle size and particle fracture on the elastic/plastic deformation of metal matrix composites. Acta Mat. 44, 3801–3811.

Nye, J.F., 1953. Some geometrical relations in dislocated crystals. Acta Metall. 1, 153–162.

Ortiz, M., Repetto, E.A., Stainier, L., 1999. A theory of subgrain dislocation structures, submitted for publication.

Peirce, D., Asaro, R.J., Needleman, A., 1983. Material rate dependence and localized deformation in crystalline solids. Acta Metall. 31, 1951–1976.

Shu, J.Y., Fleck, N.A., 1999. Strain gradient crystal plasticity: size-dependent deformation of bicrystals. J. Mech. Phys. Solids 47, 297–324.

Stölken, J.S., Evans, A.G., 1998. A microbend test method for measuring the plasticity length scale. Acta Mater. 46, 5109–5115.

Van der Giessen, E., Needleman, A., 1995. Discrete dislocation plasticity: a simple planar model. Model. Simul. Mater. Sci. Eng. 3, 689–735.